Site Selection and Capacity Determination of Electric-Hydrogen Charging Integrated Station Based on Voronoi Diagram and Particle Swarm Algorithm

Xueqin Tian , Heng Yang * , Yangyang Ge , Tiejiang Yuan

Posted Date: 25 November 2023

doi: 10.20944/preprints202311.1594.v1

Keywords: electric vehicles; hydrogen fuel cell vehicles; site selection and fixed capacity; voronoi diagram; electric-hydrogen integrated charging station

Article

Site Selection and Capacity Determination of Electric-Hydrogen Charging Integrated Station Based on Voronoi Diagram and Particle Swarm Algorithm

Xueqin Tian , Heng Yang * , Yangyang Ge , Tiejiang Yuan

Posted Date: 25 November 2023

doi: 10.20944/preprints202311.1594.v1

Keywords: electric vehicles; hydrogen fuel cell vehicles; site selection and fixed capacity; voronoi diagram; electric-hydrogen integrated charging station

Article

Site Selection and Capacity Determination of Electric-Hydrogen Charging Integrated Station Based on Voronoi Diagram and Particle Swarm Algorithm

Xueqin Tian [1,2], Heng Yang [2,*], Yangyang Ge [3] and Tiejiang Yuan [2]

[1] China Electric Power Research Institute Co.,Ltd.,Haidian District, Beijing 100192, China
[2] School of Electrical Engineering, Dalian University of Technology, Dalian, Liaoning 116024, China
[3] Electric Power Research Institute of State Grid Liaoning Electric Power Co., Ltd., Shenyang 110006, China
* Correspondence: 936570628@qq.com

Abstract: In view of the problem of charging and hydrogen filling facilities construction in the transition from fuel vehicles to electric vehicles and hydrogen fuel cell vehicles, in order to meet the electric energy demand of electric vehicles and hydrogen energy demand of hydrogen fuel cell vehicles at the same time, this paper puts forward a method of siting and capacity determination of electric-hydrogen refueling integrated station (EHRIS) based on Voronoi diagram and particle swarm algorithm based on calculating the demand of charging and filling of hydrogen in vehicles. Firstly, OD pair(Origin-Destination) is used to represent the starting point and end point of the car to portray the travel demand of the car, and on the basis of the traffic network model, the shortest driving path of the new energy car is determined by Dijkstra algorithm, and Monte Carlo simulation is used to get the electric-hydrogen energy demand of the car; secondly, the Voronoi diagram is introduced to classify the service scope of the electric-hydrogen charging station to determine the equipment capacity of the electric-hydrogen charging station, while taking into account the electric-hydrogen charging and refueling capacity. Secondly, a Voronoi diagram is introduced to divide the service scope of the EHRIS, determine the capacity of the equipment in the EHRIS, and consider the distance constraints between the sites of EHRIS, so as to make the division of the site and service scope more reasonable. Finally, a dynamic optimal current model framework for distribution networks based on second-order cone relaxation is established, and each element of the active distribution network is planned, so that the distribution network can operate safely and stably after being connected to the EHRIS. With the objective of minimizing the total social cost of EHRIS and considering the constraints of the charging equipment and hydrogen production and injection equipment of the EHRIS, a siting and capacity model to meet the electric-hydrogen energy demand of electric and hydrogen fuel cell vehicles is developed, and solved by a particle swarm algorithm. Finally, the simulation planning is carried out with Sioux Falls city and IEEE33 network, which ensures the stable operation of the power grid while meeting the energy demand of automobiles, and the results verify the effectiveness and feasibility of the proposed method.

Keywords: electric vehicles; hydrogen fuel cell vehicles; site selection and fixed capacity; voronoi diagram; electric-hydrogen integrated charging station

1. Introduction

With the large-scale use of fuel vehicles, the environmental problems caused by them have gradually attracted people's attention. In order to reduce carbon emissions from traditional fuel vehicles, realize low-carbon environmental protection, energy saving and emission reduction, it is imperative to promote the application of new energy vehicles [1]. New energy vehicles mainly include electric vehicles and hydrogen fuel cell vehicles [2].

 doi:10.20944/preprints202311.1594.v1

Hydrogen energy, as a green energy source, will play a significant role in upgrading and transforming traditional fuel vehicles and realizing a low-carbon process. Due to the actual factors such as power grid structure, vehicle energy storage capacity, and replenishment method, there are significant differences between the planning and design of EHRIS and the traditional fuel vehicle refueling station site: large-scale centralized charging of electric vehicles will impact on the power grid, affecting the frequency and voltage stability, and compared with the short-term refueling of fuel vehicles, the charging of electric vehicles takes a long time, so a reasonable site layout of the charging station is needed to avoid the centralized charging of electric vehicles. Centralized charging. With the increasing proportion of new energy vehicles, it is of great significance to carry out a study on the location and capacity of EHRIS in order to meet the energy demand of electric vehicles and hydrogen fuel cell vehicles.

For the planning study of EHRIS, firstly, the planning methodology of the charging station can be borrowed. In [3], on the basis of candidate charging station sites, charging stations are planned with the objective of minimizing the distance traveled by cars to the charging station. This approach meets the energy demand of electric its but ignores the influence of roads on the car's driving behavior. In [4], the charging station planning model is established with the objective of minimizing the cost of charging station construction and management as well as the cost of EV driving losses, but it is specific in that it considers the airport road as a one-dimensional road. In [5], considering the influence of transportation road network on electric vehicle charging demand, a two-stage method is used, in which the first stage obtains the spatial and temporal distribution of automobile electric energy demand, and the second stage establishes a model for optimal siting and capacity determination of charging stations with the objective of minimizing charging station operation and investment costs. Secondly, the planning methodology for hydrogen refueling stations can be drawn upon. In [6], the authors proposed a hydrogen network supply system for wind power generation, and the model can be used for hydrogen refueling station planning and provides a rational hydrogen infrastructure layout scheme. In [7], the authors propose a hydrogen refueling site sizing model based on the life cycle cost of hydrogen, yet only a one-dimensional highway is used as the study object, which does not have the two-dimensional characteristics of the urban transportation plane. In [8], the authors propose to establish a cross-regional transportation fuel cell vehicle hydrogen refueling station siting model based on the traffic flow capture model, which takes into account the average road vehicle speed, road traffic flow, the maximum vehicle mileage, and the maximum number of hydrogen refueling stations constructed, to obtain the hydrogen refueling station siting scheme between different regions.

Finally, for the study of an integrated electric hydrogen refueling station, authors [9] proposed a market-based power purchase strategy for EHRIS based on peak shaving and valley filling, wind and solar energy consumption and hydrogen energy supply, and verified that the integrated station effectively improves the capacity of peak shaving and valley filling and new energy consumption of the power grid. In [10], sampling on the basis of four uncertainties: wind, light, electricity, and hydrogen, to demonstrate the economy and effectiveness of capacity planning for integrated electricity-hydrogen energy stations under different scenarios. To summarize, the existing research focuses on the location and capacity of individual EV charging stations or hydrogen fuel cell vehicle refueling stations, without considering the driving characteristics of EVs and hydrogen fuel cell vehicles in the city, the lack of simultaneous supply of electricity and hydrogen and the lack of related equipment capacity planning, and the lack of research on the large-scale access to the grid for EVs and hydrogen fuel cell vehicles.

This paper proposes a planning method for EHRIS to meet the energy demand of electric vehicles and hydrogen fuel cell vehicles. Firstly, the OD travel matrix is used to portray the transportation demand, and then the Dijkstra's algorithm is used to plan the shortest driving paths of the vehicles to calculate the electric energy demand of electric vehicles and the hydrogen energy demand of hydrogen fuel cell vehicles. Secondly, the Voronoi diagram is used to divide the service area of each EHRIS site and determine the equipment capacity of EHRIS. Finally, simulation planning

 doi:10.20944/preprints202311.1594.v1

with the city of Sioux Falls and the IEEE33 network ensures stable operation of the grid while meeting the energy demand of electric vehicles and hydrogen fuel cells.

2. Framework for the operation of EHRIS

This paper proposes an integrated electric-hydrogen manufacturing and charging station, which refers to a place to provide hydrogen energy for electric vehicles and hydrogen fuel cell vehicles. Due to the rapid development of hydrogen energy system [11], the electric-hydrogen manufacturing and charging station can realize the energy management of distribution grid, distributed energy, hydrogen manufacturing and storage on the source side, and realize the coordination and optimization of electric vehicles and hydrogen fuel cell vehicles on the load side, so as to achieve the purpose of energy saving and emission reduction in transportation.

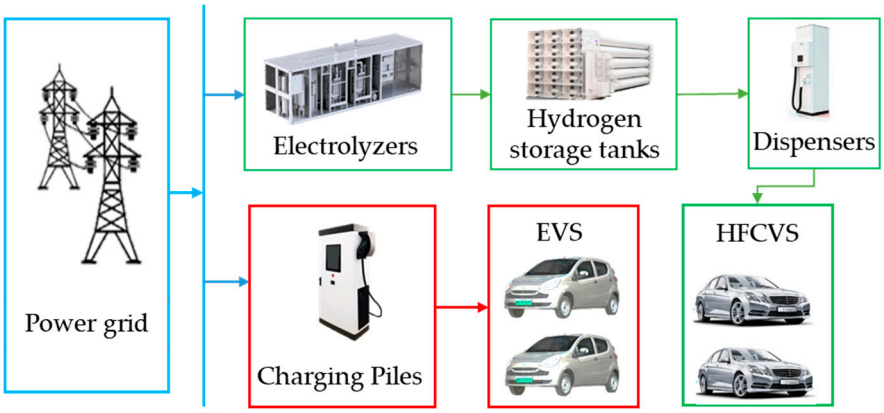

Figure 1. Framework for the operation of EHRIS.

Electric vehicle fast charging device realizes fast charging of electric vehicles [12]，Hydrogen energy system includes hydrogen production unit, hydrogen storage unit and hydrogen refueling unit. Hydrogen production device consists of an electrolyzer, which electrolyzes water through electrodes to obtain hydrogen and oxygen. At the present stage, the hydrogen production project mainly adopts proton exchange membrane and alkaline electrolyzer, which is highly flexible and adaptable. It can operate stably and safely at high current density and low voltage. In this paper, alkaline electrolyzer is used to produce hydrogen with high pressure gaseous storage hydrogen storage tank [13].

3. Automotive Electric Hydrogen Demand Model

Electric vehicles consume electric energy while traveling, and the corresponding hydrogen fuel cell vehicles consume hydrogen energy. Calculation and simulation of the energy demand of electric vehicles and hydrogen fuel cell vehicles is the basis for siting and capacity determination of the electric-hydrogen charging station.

3.1. Transportation Network Model

Transportation network as an important carrier of new energy vehicle driving [14], its topology has an important impact on the driving path of new energy vehicles, through the graph theory [15] can establish the transportation road network model to portray the characteristics of the road network, Figure 2 shows the topology of the transportation road network.

 doi:10.20944/preprints202311.1594.v1

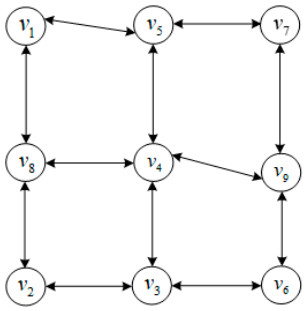

Figure 2. Traffic Network Topology.

The mathematical description of the transportation road network is shown in equation (1):

$$\begin{aligned} &G=(V,E,K,W)\\ &V=\{v_i|\ i=1,2,3,\cdots,n\}\\ &E=\{v_{ij}|\ v_i\in V,v_j\in V,i\neq j\}\\ &K=\{k|\ k=1,2,3,\cdots,m\}\\ &W=\{w_{ij}^k|\ v_{ij}\in E,k\in K\} \end{aligned} \tag{1}$$

where G is the traffic network; V denotes the traffic intersection; E denotes the traffic section; W is the roadway resistance; and K denotes the m time periods throughout the day.

The structure of the traffic road network in Figure 2 is represented using the adjacency matrix A:

$$A=\begin{bmatrix} A_{11} & A_{12} & \cdots & A_{1N}\\ A_{21} & A_{22} & \cdots & A_{2N}\\ \vdots & \vdots & \ddots & \vdots\\ A_{M1} & A_{M2} & \cdots & A_{MN} \end{bmatrix} \tag{2}$$

The assignment rule for the element a_{ij} in matrix A is as follows:

$$a_{ij}=\begin{cases} w_{ij}, & v_{ij}\in E\\ 0, & v_i=v_j\\ \text{inf}, & v_{ij}\notin E \end{cases} \tag{3}$$

where: inf denotes that there is no directly connected road section between node v_i and v_j; w_{ij} denotes the road resistance from node v_i to v_j.

Considering the fact that users are actually more concerned about the car traveling time while driving[16] .Therefore, this study chooses car travel time as a characterization of roadway resistance for modeling and analysis.

3.2. New Energy Vehicle Charging and Hydrogen Injection

3.2.1. Road resistance function

When making path selection, the route with the shortest traveling time is preferred. In order to reflect the relationship between the traffic time and the density of each road segment and other factors, this paper adopts the road resistance function method. The road resistance function is often calculated according to the following formula[17] :

$$T_{at}(x_{at})=T_{at}^0[1+\alpha(x_{at}/C_a)^\beta] \tag{4}$$

where T_{at}^0 denotes the free passage time of section a; C_a is the capacity of line a; x_{at} denotes the flow rate of section a at time t; $\alpha=0.15$, $\beta=4$; ;

 doi:10.20944/preprints202311.1594.v1

3.2.2. Vehicle path planning

In order to simulate the travel demand of electric vehicles and hydrogen fuel cell vehicles, the OD matrix representation of traffic origins and destinations is used [18] , and (m, n) is defined as an OD pair, where m denotes the user's starting point, n denotes the ending point, and M denotes the set of OD pairs.

$$M = \begin{bmatrix} M_{11} & M_{12} & \cdots & M_{1n} \\ M_{21} & M_{22} & \cdots & M_{2n} \\ \vdots & \vdots & \ddots & \vdots \\ M_{m1} & M_{11} & \cdots & M_{mn} \end{bmatrix} \quad (5)$$

where M_{mn} is the traffic flow from intersection m to intersection n;

3.2.3. EV Electricity Demand and HFCV Hydrogen Demand Calculation

1) Firstly, we obtain urban traffic information including traffic network structure and road resistance, and read the travel demand of electric vehicles and hydrogen fuel cell vehicles, including the travel moments, starting points and ending points of electric vehicles and hydrogen fuel cell vehicles, the initial power quantity of electric vehicles and the initial hydrogen quantity of hydrogen fuel cell vehicles. State parameters for electric vehicles $EV = \{EO_i, ED_i, Et_s, EL_t, ECap_r\ ECap_0, ECap_t, E\Delta cap\}$;state parameters for hydrogen fuel cell vehicles $HFCV = \{FO_i, FD_i, Ft_s, FL_t, FCap_r, FCap_0, FCap_t, F\Delta cap\}$, The meaning of each parameter is shown in Table 1.

Table 1. Car state Parameters.

Parameter	Explanation	Parameter	Explanation
EO_i	Electric Vehicle Starting Point	Et_s	Electric car travel time
ED_i	Electric Vehicle Endpoints	EL_t	Position of the electric car at time t
$ECap_r$	Electric Vehicle Capacity	$ECap_0$	Initial power of electric vehicles
$ECap_t$	Amount of power remaining in the electric car at time t	$E\Delta cap$	Consumption per kilometer Electricity consumption
FO_i	Hydrogen Fuel Cell Vehicle Starting Point	FD_i	Hydrogen Fuel Cell Vehicle Endpoint
Ft_s	Hydrogen fuel cell vehicle position at time t	FL_t	Hydrogen fuel cell vehicle position at time t
$FCap_r$	Hydrogen fuel cell vehicle hydrogen content	$FCap_0$	Initial Hydrogen for Hydrogen
$FCap_t$	Amount of hydrogen remaining in the hydrogen fuel cell vehicle at time t	$F\Delta cap$	Hydrogen consumption per kilometer

In this paper, we use the probability distribution curves of the initial travel moments and return moments of cars on a typical weekday provided in the literature [19] to generate the initial travel moments of electric cars and hydrogen fuel cell cars. Assuming [20] that the initial power of each electric vehicle and the initial hydrogen energy distribution of hydrogen fuel cell vehicles satisfy normal distribution on a day satisfy the normal distribution $N(0.5, 0.1^2)$.

2)Complementary energy demand judgment and user decision-making

After the vehicle has traveled to a certain intersection, the user determines whether it needs to replenish energy to travel to the destination based on the remaining power and hydrogen of the vehicle. In this paper, it is assumed that if the electric car's power or hydrogen fuel cell car's hydrogen amount is less than 20% or the remaining energy of the car is not enough to reach the destination, the car needs to go to the charging station at the current intersection to replenish the energy. When the car continues to its destination after refueling, the cost of loss between the car and the refueling station will be calculated as part of the planning cost of the refueling station.

$$\zeta_i^s = \begin{cases} 1 & S(i_s) \le 20\% \text{ or } L_R(i_s) \le L_{s,D} \\ 0 & \text{other} \end{cases} \quad (6)$$

where ζ_i^s function determines whether the ith car needs to be charged and injected with hydrogen when it travels to s, 1 indicates that the car needs to be replenished, and 0 indicates that it does not

 doi:10.20944/preprints202311.1594.v1

need to be replenished; $S(i_s)$ is the remaining energy of the car when it arrives at the intersection s; $L_R(i_s)$ is the mileage that can be traveled with the remaining power and hydrogen in kilometers, and $L_{s,D}$ is the distance between the current intersection node s and the destination in kilometers.

3)Based on Dijkstra's shortest path planning

After the EV and HFCV obtain the traveling OD pair, in order to get the shortest driving path planned by the EV and HFCV users, this paper adopts the Dijkstra algorithm to guide the users on the path[21] , which takes the shortest driving path as the searching goal by filtering and comparing the road paths.

$$S_{ij} = \sum_{v_{ij} \in E} \left[v_{ij} w_{ij}^{k}(t) \right] \tag{7}$$

$$v_{ij} = \begin{cases} 1, & v_{ij} \in d_m(i) \\ 0, & v_{ij} \notin d_m(i) \end{cases} \tag{8}$$

where $v_{ij} = 1$ indicates that the road from node i to node j is in the actual traveling path $d_m(i)$, otherwise it is 0; therefore, the starting point $O(i)$ and the ending point $D(i)$, as well as the initial traveling moment $t_0(i)$ and the returning moment $t_d(i)$ are obtained through the OD travel matrix and the traveling path is planned by the Dijkstra's algorithm; dm simulates the vehicle EV/HFCV traveling route.

4)Calculation of electro-hydrogen demand

The driving paths and replenishment needs of all electric vehicles and hydrogen fuel cell vehicles in the planning area are modeled according to the aforementioned method, and the charging and hydrogen injection quantities of all electric vehicles and hydrogen fuel cell vehicles in a day are superimposed and calculated to obtain the electric hydrogen demand of all electric vehicles in the planning area. The flow chart for total demand calculation is as follows：

4. Site selection for capacity determination based on Voronoi diagram with particle swarm algorithm

4.1. The steps for selecting the initial site for EHRIS

1) Calculate the electric and hydrogen energy demand of automobiles at each transportation node;

2) Randomly generate N EHRIS site coordinates in the planning area and compile them as the initial particle X;

3) Generate a Voronoi diagram [22] with each initial station site as a growth kernel, and the area formed by the growth is the service area of each charging station;

4) Using the investment and construction cost of EHRIS and the user's refueling loss cost as the site selection and capacity model, the particle swarm algorithm determines the optimal site distribution.

4.2. Voronoi diagram based on the division of the scope of service of the integrated hydrogen refueling station

The division of the service area of EHRIS is a prerequisite for realizing the capacity allocation of EHRIS. The Voronoi diagram, also known as the Tyson polygon or Dirichlet diagram, consists of a set of consecutive polygons consisting of the perpendicular bisectors connecting the straight lines of the two neighboring points. The EHRIS as a generating element, and make the vertical bisectors connecting the line segments, the intersection line between these vertical bisectors will form some polygons, so that the whole plane is divided into some sub-areas, through the Voronoi diagram divided into each area to establish an EHRIS, when the car energy is insufficient to drive to the charging station to replenish the energy in a timely manner.

Let the set of vertices in the $P = \{p_1, p_2, \cdots, p_n\}$, $3 \le n \le \infty$, $d(p_i, p_j)$ be the Euclidean distance between vertices p_i and p_j. The Voronoi diagram is defined as:

 doi:10.20944/preprints202311.1594.v1

$$V(p_i,\lambda_i)=\left\{x\in V(p_i,\lambda_i)|\ d(x,p_i)\le d(x,p_j)\right\},\quad j=1,2,\cdots,n,j\ne i \tag{9}$$

The Voronoi diagram divides the plane into n regions, and each vertex in P corresponds to a $V(p_i,\lambda_i)$ region. When the car needs to replenish energy, it drives to the nearest EHRIS, and its service range is determined by the Voronoi diagram.

5. Siting and capacity modeling of an EHRIS

The Hydrogen Charging Station supplies energy to both electric vehicles and hydrogen fuel cell vehicles. The station includes transformers, charging piles, electrolysis tanks, hydrogen storage tanks, hydrogen dispensers and other equipment, and uses alkaline electrolyzed water to produce hydrogen in the station. Among them, the charging piles are used to replenish the energy of electric vehicles, while the electrolysis tank, hydrogen storage tank and hydrogen dispenser are used to produce hydrogen and dispense hydrogen to hydrogen fuel cell vehicles [23].

5.1. Objective function

The objective function for the construction of an electric-hydrogen charging station, which is a transportation infrastructure that provides services to users for travel, is the cost of constructing an electric-hydrogen charging station over the entire planning period discounted to the annual cost, and the total cost includes non-energy costs C_{1i}、C_{2i} and energy costs C_{3i}、C_{4i}:

$$\min C=\sum_{i=1}^{N}\left(C_{1i}+C_{2i}+C_{3i}+C_{4i}\right) \tag{10}$$

where C is the cost of constructing electric-hydrogen refueling stations over the entire planning period discounted to each year; N is the number of refueling stations;

The individual costings are shown below:

1) C_{1i} is the annual cost of the investment in the construction of the integrated hydrogen refueling station：

$$C_{1i}=\frac{r_0(1+r_0)^z}{(1+r_0)^z-1}\begin{pmatrix}e_ia_1+u_ib_1+v_ib_2+\\ h_ic_2+w_id_2+c_i\end{pmatrix} \tag{11}$$

where e_i is the number of transformers in the EHRIS; a_1 is the unit price of the transformers; u_i is the number of charging piles in the EHRIS; b_1 is the unit price of the charging piles in the EHRIS; v_i is the number of hydrogen dispensers in the EHRIS; b_2 is the unit price of the hydrogen dispensers in the EHRIS; h_i is the capacity of the hydrogen tanks in the EHRIS; c_2 is the price per unit of the hydrogen tanks in the EHRIS Price per unit capacity of hydrogen storage tanks in the EHRIS; w_i is number of electrolyzes in the EHRIS i; d_2 is unit price of electrolyzes in the EHRIS; c_i is the capital cost of the EHRIS i; r_0 is the discount rate; z is the operating life of the EHRIS i.

2) The maintenance cost C_{2i} of the EHRIS consists mainly of the cost of repairing the equipment of the EHRIS and the cost of labor for the personnel. The maintenance cost is calculated as a percentage of the construction cost, with a scaling factor of η. The annual maintenance cost of the EHRIS i will be:

$$C_{2i}=\eta\begin{pmatrix}e_ia_1+u_ib_1+v_ib_2+\\ h_ic_2+w_id_2+c_i\end{pmatrix} \tag{12}$$

3) C_{3i} is the cost of purchasing electricity for the EHRIS i and the cost of electricity consumption for hydrogen production in the electrolyzer:

$$C_{3i}=\sum_{t=1}^{T}\left(P_{i,t,cd}^{sum}+P_{i,\,t,\mathrm{elec}}^{sum}\right)\times p_{t,0} \tag{13}$$

where $p_{t,0}$ is the purchased electricity price of the electric-hydrogen charging station in time period t; $P_{i,cd}^{sum}$ is the sum of the electricity required by the charging piles in the service area of the electric-

 doi:10.20944/preprints202311.1594.v1

hydrogen charging station; $P_{i,\text{elec}}^{sum}$ is the sum of the electricity consumed by the electrolyzer for hydrogen production;

4) C_{4i} is the cost of idling energy loss incurred by the user during the journey to the electric hydrogen refueling integrated station, which is expressed as a function of:

$$C_{4i} = \frac{\sum L_{i,ev}}{g_{ev}} \times p_0 + \frac{\sum L_{i,hev}}{g_{hev}} \times h_0 \tag{14}$$

where $\sum L_{i,ev}$ and $\sum L_{i,hev}$ are the combined distances from all traffic intersections within the service area of electric-hydrogen charging station i to the EVs and hydrogen fuel cell vehicles at EHRIS i, respectively; g_{ev} and g_{hev} are the electricity and hydrogen consumed per kilometer by EVs and fuel cell vehicles, respectively;

5.2. Determination of the number of hydrogen dispensers for charging piles at electric hydrogen charging stations

If in time period t, if there are n_i demand points within the service area of the EHRIS i, the number of charging piles and hydrogen dispensers in the EHRIS is configured as follows:

Number of charging piles:

$$u_i = \left[\frac{\sum_{j=1}^{n_i} {q_{ev,t}}^j (\rho_1 + 1)}{P_1 k_{1,x}} \right] \tag{15}$$

Number of hydrogenators:

$$v_i = \left[\frac{\sum_{j=1}^{n_i} {M_{hfcv,t}}^j (\rho_2 + 1)}{P_2 k_{2,x}} \right] \tag{16}$$

where ρ_1 is the charging margin of the EHRIS; P_1 is the rated power of each charging pile; $k_{1,x}$ is the charging efficiency of the charging pile; ρ_2 is the hydrogen injection margin of the hydrogen dispenser in the EHRIS; P_2 is the rated hydrogen injection capacity of a single hydrogen dispenser; $k_{2,x}$ is the hydrogen injection efficiency of the hydrogen dispenser; ${q_{ev,t}}^j$ denotes the demand for electric loads of EVs in the service area of the EHRIS i at time t; ${M_{hfcv,t}}^j$ denotes the demand for hydrogen of HFCVS in the service area of the EHRIS i at time t; and [] is the sign of upward rounding.

5.3. Constraints

The constraints include a limit on the number of EHRIS, a limit on the number of EHRIS, a constraint on the distance between EHRIS, and a constraint on the distance from a traffic intersection to an EHRIS:

1) Electrolyzer hydrogen production constraints:

The electrolyzer consumes electricity to produce hydrogen:

$$P_{i,\text{elec}}^{t,d} = H_{\text{H}} \frac{F_{i,\text{elec}}^{t,d}}{\eta_{\text{elec}}} \tag{17}$$

$$w_i = \text{ceil}\left[\frac{\sum_{j=1}^{n_i} \sum_{t=1}^{24} P_{\text{elec},t}^{j}}{P_{\text{elec}}} \right] \tag{18}$$

$$0 \le F_{i,\text{elec}}^{t,d} \le \Gamma_{i,\text{elec}} \tag{19}$$

 doi:10.20944/preprints202311.1594.v1

$$\underline{\Gamma_{i,\text{elec}}} \le \Gamma_{i,\text{elec}} \le \overline{\Gamma_{i,\text{elec}}} \tag{20}$$

where $P_{i,\text{elec}}^{t,d}$ is the input power of the electrolyzer at time t on day d of the year in EHRIS i; H_{H} is the high calorific value of hydrogen; $F_{i,\text{elec}}^{t,d}$ is the hydrogen productivity of the electrolyzer at time t on day d of the year in EHRIS i; η_{elec} is the energy conversion efficiency of the electrolyzer; $\Gamma_{i,\text{elec}}$ is the hydrogen production capacity of the electrolyzer in EHRIS i; and $\underline{\Gamma_{i,\text{elec}}}$ and $\overline{\Gamma_{i,\text{elec}}}$ denote the lower and upper limits of the hydrogen production rate of the electrolyzer in EHRIS i, respectively;

2) Hydrogen storage tank capacity constraints：

Hydrogen produced in the electrolyzer is not immediately consumed by the fuel cell vehicle immediately, but is stored in a hydrogen storage tank.

$$C_{i,\text{tank}}^{t+1,d} = C_{i,\text{tank}}^{t,d} - M_{i,\text{out}}^{t,d} + F_{i,\text{elec}}^{t,d} \tag{21}$$

where $C_{i,\text{tank}}^{t,d}$ and $C_{i,\text{tank}}^{t+1,d}$ are the hydrogen storage capacity in the hydrogen storage tank at time t and t+1 on day d, respectively; $M_{i,\text{out}}^{t,d}$ is the hydrogen storage capacity in the hydrogen storage tank at time t on day d; and $F_{i,\text{elec}}^{t,d}$ is the hydrogen inflow from the hydrogen dispenser to the hydrogen storage tank at time t on day d in the hydrogen storage tank in the EHRIS;

$$0 \le C_{i,\text{tank}}^{t,d} \le h_i \tag{22}$$

$$\underline{h_i} \le h_i \le \overline{h_i} \tag{23}$$

where h_i is the capacity of the hydrogen storage tank; $\underline{h_i}$ is the lower limit of the rated hydrogen storage capacity of hydrogen storage tank i of the electric hydrogen refueling station; $\overline{h_i}$ is the upper limit of the rated hydrogen storage capacity of hydrogen storage tank i of the electric hydrogen refueling station;

3) Number of electric hydrogen refueling stations constraints

$$N_{\min} \le N \le N_{\max} \tag{24}$$

where $N_{\min}$ and $N_{\max}$ are the minimum and maximum values of the number of EHRIS allowed to be built in the planning area.

4) Distance constraints between EHRIS

$$D_{\min} \le D_{ij} \le D_{\max} \quad i \ne j \tag{25}$$

where D_{ij} is the straight line distance between EHRIS i and hydrogen charging station j; $D_{\min}$ and $D_{\max}$ are the minimum and maximum distances between EHRIS i and EHRIS j, respectively.

5) Distance constraints from traffic intersections to EHRIS

$$d_{ij} \le d_{\max} \tag{26}$$

where d_{ij} is the distance from the EHRIS to the traffic demand point; $d_{\max}$ is the maximum distance from the traffic demand point to the EHRIS; N_{cross} is the number of traffic intersections.

5.4. Improved Particle Swarm Algorithm

Because the EHRIS siting and capacity model contains variables such as charging piles, hydrogen refueling stations, the distance between the EHRIS and the demand point of automobile refueling, and the charging equipment and hydrogen refueling equipment in the EHRIS, which is difficult to be solved by using the conventional mathematical methods, this paper adopts the improved particle swarm algorithm based on the division of the Voronoi diagram [24] for the model of the EHRIS.

5.4.1. Weighting update strategy

In this paper, the inertia weights in the traditional particle swarm algorithm are improved to solve the problems of easy to fall into local optimum at the beginning of iteration and easy to oscillate at the end of iteration [25], and the inertia weights w, are updated in each iteration. When the inertia

 doi:10.20944/preprints202311.1594.v1

weight is large, the particle has a strong ability in global search, but at the same time the adaptation update rate is slow; when the inertia weight w is small, the algorithm is strong in local region search, but it is easy to fall into local optimal solutions. Therefore, this paper adopts the linear decreasing strategy [26] to update w, and the specific update formula is:

$$w = w_{\max} - \frac{T \cdot (w_{\max} - w_{\min})}{T_{\max}} \tag{27}$$

where $w_{\max}$ and $w_{\min}$ are the maximum and minimum values of the inertia weights, respectively; T and $T_{\max}$ are the current and maximum iterations, respectively.

5.4.2. Solution process

The solution flow chart of the electric-hydrogen charging and injecting integrated station is shown in Figure 3, which is mainly divided into the following seven steps:

Step 1: Calculate the electricity and hydrogen demand of urban transportation nodes based on the start and end of electric vehicle and hydrogen fuel cell vehicle trips in the planning area.

Step 2: Generate the coordinates of the site of the EHRIS, and compile them into the initial location of the EHRIS.

Step 3: Make a Voronoi diagram with the initial site of the EHRIS as the growth point to determine the service area of each EHRIS, and determine the number of charging piles and hydrogen dispensers according to the electricity and hydrogen load demand within the service area;

Step 4: Calculate the annual social cost of the EHRIS according to the objective function of planning, use it as the adaptation degree, and finally find the individual extreme value of the particle and the global extreme value.

Step 5: Judge whether the maximum number of iterations is reached. Yes, go to step 7; No, execute step 6.

Step 6: Update the velocity and position of the particle, jump to step 3, iteration number 1.

Step 7: Output the planning scheme that minimizes the objective function.

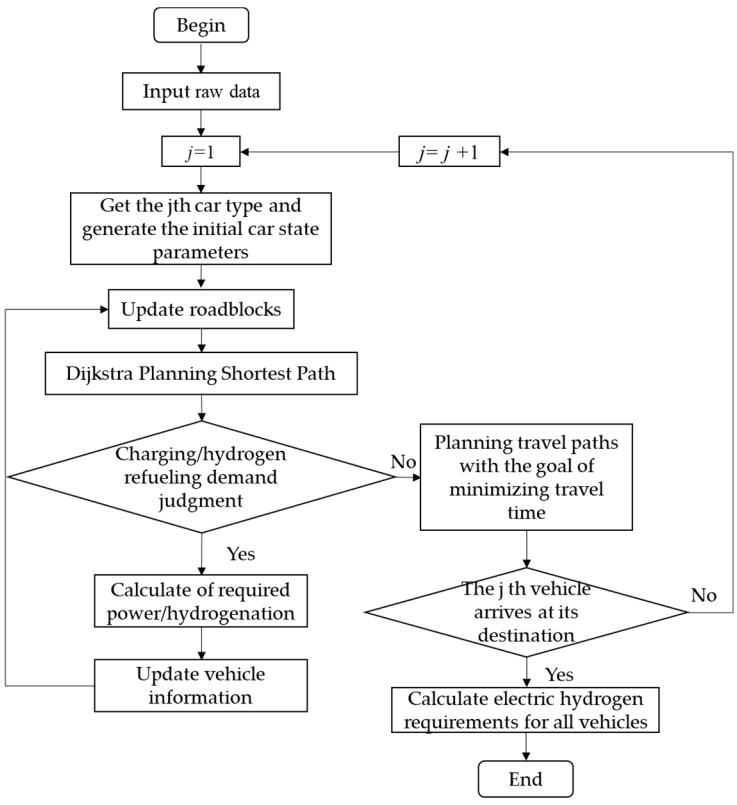

Figure 3. Calculation flow chart of hydrogen injection load for vehicle charging.

 doi:10.20944/preprints202311.1594.v1

5.5. Grid Planning for Combined Electric Hydrogen Charging Station

In the case of electric hydrogen charging integrated station access, in order to make the safe and stable operation of the power grid, the active distribution network expansion planning is established, and the active distribution network management factors include [27]: 1) on-load voltage regulating power transformer (on-load tap changer (OLTC)); 2) reactive power device regulation, including discrete reactive power compensation and continuous reactive power regulation; and 3) energy storage system (ESS). storage system (ESS). Synthesizing the electric hydrogen production and charging integrated station and management factors, this paper adopts the optimal current model of distribution network from literature [28]:

$$\min f(p,q,P,Q,\tilde{V},\tilde{I})$$

$$s.t.\begin{cases} p_j = \sum_{k\in\delta(j)} P_{jk} - \sum_{i\in\pi(j)} (P_{ij} - \tilde{I}_{ij} r_{ij}) + g_j \tilde{V}_j, \quad \forall j \in B \\ q_j = \sum_{k\in\delta(j)} Q_{jk} - \sum_{i\in\pi(j)} (Q_{ij} - \tilde{I}_{ij} x_{ij}) + b_j \tilde{V}_j, \quad \forall j \in B \end{cases} \tag{28}$$

$$\widetilde{V_j} = \widetilde{V_i} - 2(P_{ij} r_{ij} + Q_{ij} x_{ij}) + \widetilde{I_{ij}}(r_{ij}^2 + x_{ij}^2), \quad \forall ij \in E \tag{29}$$

$$\left\| \begin{matrix} 2P_{ij} \\ 2Q_{ij} \\ \tilde{I}_{ij} - \tilde{V}_j \end{matrix} \right\|_2 \le \tilde{I}_{ij} + \tilde{V}_j, \quad \forall ij \in E \tag{30}$$

$$\underline{I_{ij}^2} \le \tilde{I}_{ij} \le \overline{I_{ij}^2}, \quad \forall ij \in E \tag{31}$$

$$\underline{V_j^2} \le \tilde{V}_j \le \overline{V_j^2}, \quad \forall j \in B^+ \tag{32}$$

6. Active Management Element Modeling

6.1. OLTC modeling

OLTC mainly regulates the HV/MV low-voltage side voltage value. With the addition of OLTC, the substation bus node is converted into an adjustable variable, which can be replaced as follows:

$$\begin{cases} \underline{V_j^2} \le (V_{j,t}^{\text{Base}})^2 r_{j,t} \le \overline{V_j^2} \\ r_j^{\min} \le r_{j,t} \le r_j^{\max} \end{cases}, \quad \forall t, \forall j \in B^{\text{OLTC}} \tag{33}$$

where B^{OLTC} is the set of substation nodes containing the OLTC; $V_{j,t}^{Base}$ is the voltage value of the high voltage side of the HV/MV transformer, which is constant; r_j^{max} and $r_j^{\min}$ are the squares of the upper and lower limits of the OLTC's adjustable ratios; and $r_{j,t}$ is the square of the OLTC's ratios, which is defined as the ratio of the secondary to the primary side, and is actually a discrete-valued variable, which can be further processed into the following relationship containing 0-1 variables:

$$r_{j,t} = r_j^{\min} + \sum_s r_{j,s} \sigma_{j,s,t}^{\text{OLTC}}, \quad \forall t, \forall j \in B^{\text{OLTC}} \tag{34}$$

where $r_{j,s}$ denotes the difference between the OLTC gear s and the square of the variable ratio of gear s-1, i.e., the neighboring regulation increment. $\sigma_{j,s,t}^{\text{OLTC}}$ is a 0-1 identifying variable, which can be further constrained to be if the constraints such as the limit on the number of regulation times are considered to be imposed in practice:

 doi:10.20944/preprints202311.1594.v1

$$\begin{cases} \sigma_{j,1,t}^{\mathrm{oLTC}} \geq \sigma_{j,2,t}^{\mathrm{oLTC}} \geq \sigma_{j,\mathrm{SR}_j,t}^{\mathrm{oLTC}}, \quad \forall t, \forall j \in B^{\mathrm{OLTC}} \\ \delta_{j,t}^{\mathrm{OLTC,IN}} + \delta_{j,t}^{\mathrm{OLTC,DE}} \leq 1, \quad \forall t, \forall j \in B^{\mathrm{OLTC}} \\ \sum_s \sigma_{j,s,t}^{\mathrm{OLTC}} - \sum_s \sigma_{j,s,t-1}^{\mathrm{OLTC}} \geq \delta_{j,t}^{\mathrm{OLTC,N}} - \delta_{j,t}^{\mathrm{OLTC,DE}} \mathrm{SR}_j, \\ \qquad \forall t, \forall j \in B^{\mathrm{OLTC}} \\ \sum_s \sigma_{j,s,t}^{\mathrm{OLTC}} - \sum_s \sigma_{j,s,t-1}^{\mathrm{OLTC}} \leq \delta_{j,t}^{\mathrm{OLTC,IN}} \mathrm{SR}_j - \delta_{j,t}^{\mathrm{OLTC,DE}}, \\ \qquad \forall t, \forall j \in B^{\mathrm{OLTC}} \\ \sum_{t \in T} (\delta_{j,t}^{\mathrm{OLTC,IN}} + \delta_{j,t}^{\mathrm{OLTC,DE}}) \leq N_j^{\mathrm{OLTC,max}}, \forall j \in B^{\mathrm{OLTC}} \end{cases} \tag{35}$$

where $\delta_{j,t}^{\mathrm{OLTC,IN}}$ and $\delta_{j,t}^{\mathrm{OLTC,DE}}$ indicate the OLTC gear adjustment change identification, for 0-1 variables, if $\delta_{j,t}^{\mathrm{OLTC,IN}} = 1$, then the OLTC gear value in the t time period than the t-1 time period gear value is larger, the variable $\delta_{j,t}^{\mathrm{OLTC,DE}}$ is similar; $\mathrm{SR}_j^{\mathrm{OLTC}}$ is the maximum change range of the gear; $N_j^{\mathrm{OLTC,max}}$ is the maximum permissible number of adjustments of the OLTC gear in the T time period.

6.2. Modeling of reactive power regulation devices

1)Discrete reactive power compensation modeling. Take the example of group switching capacitor banks (CB).

$$\begin{cases} Q_{j,t}^{\mathrm{CB}} = y_{j,t}^{\mathrm{CB}} Q_j^{\mathrm{CB,step}} \\ y_{j,t}^{\mathrm{CB,max}} \leq Y_j^{\mathrm{CB,max}} \end{cases}, \quad \forall t, \forall j \in B^{\mathrm{CB}} \tag{36}$$

where B^{CB} is the set of CB nodes; $y_{j,t}^{\mathrm{CB}}$ is the number of operating groups, which is the value of discrete variable; $Y_j^{\mathrm{CB,max}}$ is the upper limit of the number of CB groups connected to node j; $Q_j^{\mathrm{CB,step}}$ is the compensated power of each group of CBs. Considering factors such as equipment life or economy, discrete reactive power compensation is mostly limited by the number of adjustments, so it generally includes a limit on the total number of operations in multiple time periods; $N_j^{\mathrm{CB,max}}$ is the upper limit of the number of operations:

$$\sum_{t \in T} | y_{j,t}^{\mathrm{CB}} - y_{j,t-1}^{\mathrm{CB}} | \leq N_j^{\mathrm{CB,max}}, \quad \forall t, \forall j \in B^{\mathrm{CB}} \tag{37}$$

Then it is available:

$$\delta_{j,t}^{\mathrm{CB}} = | y_{j,t}^{\mathrm{CB}} - y_{j,t-1}^{\mathrm{CB}} | \tag{38}$$

$$\begin{cases} \sum_{t \in T} \delta_{j,t}^{\mathrm{CB}} \leq N_j^{\mathrm{CB,max}} \\ -\delta_{j,t}^{\mathrm{CB,max}} \leq y_{j,t}^{\mathrm{CB}} \leq \delta_{j,t}^{\mathrm{CB,max}} Y_j^{\mathrm{CB,max}} \end{cases}, \quad \forall t, \forall j \in B^{\mathrm{CB}} \tag{39}$$

2) Modeling of continuous reactive power regulation devices. Take static VAR compensation (SVC) device as an example. Continuous reactive power regulation is relatively simple compared to discrete reactive power compensation devices.

$$Q_j^{\mathrm{SVC,min}} \leq Q_{j,t}^{\mathrm{SVC}} \leq Q_j^{\mathrm{SVC,max}}, \quad \forall t, \forall j \in B^{\mathrm{SVC}} \tag{40}$$

where B^{SVC} is the set of nodes containing SVC; $Q_j^{\mathrm{SVC,min}}$ and $Q_j^{\mathrm{SVC,max}}$ are the lower and upper limits of SVC compensation power, respectively. With the increasing penetration of DGs such as PV power generation, it may cause system current reversal and over-voltage problems, so the lower limit of SVC compensation in this paper $Q_j^{\mathrm{SVC,min}} < 0$.

 doi:10.20944/preprints202311.1594.v1

6.3. Modeling of energy storage devices

Typically, the energy storage device needs to consider the constraint limitations of multiple time periods, which mainly contain the charging and discharging state limitations, the charging and discharging power limitations, and the energy storage capacity constraints.

1) Charge and Discharge State constraint

$$u_{j,t}^{\text{discharge}} + u_{j,t}^{\text{charge}} \le 1, \quad \forall j \in B^{\text{ESS}}, \forall t \qquad (41)$$

2). Power constraint

$$\begin{cases} u_{j,t}^{\text{discharge}} P_j^{\text{discharge,min}} \le P_{j,t}^{\text{discharge}} \le u_{j,t}^{\text{discharge}} P_j^{\text{discharge,max}} \\ u_{j,t}^{\text{charge}} P_j^{\text{charge,min}} \le P_{j,t}^{\text{charge}} \le u_{j,t}^{\text{charge}} P_j^{\text{charge,max}} \end{cases}, \forall t, \forall j \in B^{\text{ESS}} \qquad (42)$$

3) Capacity constraint

$$\begin{cases} E_{j,t+1}^{\text{ESS}} = E_{j,t}^{\text{ESS}} + \alpha_j^{\text{charge}} P_{j,t}^{\text{charge}} - \alpha_j^{\text{discharge}} P_{j,t}^{\text{discharge}} \\ E_j^{\text{ESS,min}} \le E_{j,t}^{\text{ESS}} \le E_j^{\text{ESS,max}} \end{cases}, \forall j \in B^{\text{ESS}}, \forall t \qquad (43)$$

where B^{ESS} is the set of nodes containing ESS; Eq.(43) indicates that ESS cannot be charged and discharged at the same time, $u_{j,t}^{\text{charge}}$ and $u_{j,t}^{\text{discharge}}$ are the ESS charging and discharging states; $P_j^{\text{discharge,max}}$、$P_j^{\text{charge,max}}$、$P_j^{\text{charge,min}}$ and $P_j^{\text{discharge,min}}$ are the upper and lower limits of the ESS charging and discharging power, respectively; $E_{j,t}^{\text{ESS}}$ is the ESS power in the t time period, $E_j^{\text{ESS,max}}$ and $E_j^{\text{ESS,min}}$ is the upper and lower limits of the ESS taking into account the ESS lifetime, etc.; α_j^{charge} and $\alpha_j^{\text{discharge}}$ is the charging and discharging efficiency coefficients, in general, $\alpha_j^{\text{charge}} < 1$ and $\alpha_j^{\text{discharge}} > 1$.

Based on the comprehensive consideration of the active management element modeling, the coordination planning of the hydrogen charging station with the distribution grid is carried out based on the geographic characteristics of the planning area of the hydrogen charging station.

7. Algorithm analysis

7.1. Electricity-hydrogen demand calculations

In this paper, 24 nodes Sioux Falls are selected to describe the urban road network structure, the specific network topology is shown in Figure 4. The road network structure for automobile travel includes 24 nodes and 38 roads. The starting point of the car is set to have 2000 electric cars and 1000 hydrogen fuel cell cars in the transportation network, the rated capacity of the electric car is set to 60kWh, and the capacity of the hydrogen fuel cell car is 4kg, and the time-sharing tariff is shown in the Appendix Table A1 [29] .Where $a_1 = 80000¥$, $a_2 = 400000¥$, $b_1 = 150000¥$, $b_2 = 300000¥$, $c_2 = 9261¥$ /kg, $d_2 = 22000¥$, $c_i = 180000¥$, $z = 20$, $r_0 = 0.8\%$, $\eta = 0.05$, $\eta_{\text{elec}} = 0.73$, $h_0 = 54$ ¥/kg, $g_{ev} = 0.16kWh/km$, $g_{hev} = 0.118kg/km$, $\rho_1 = \rho_2 = 0.1$, $P_1 = 48kW/h$, $P_2 = 700kg/day$, $P_{elec} = 39kWh/kg$ $H_{\text{H}} = 3.509kW \cdot h/m^3$ .Monte Carlo sampling was used to calculate the spatial and temporal distribution of electric energy demand and hydrogen energy demand in the transportation network by searching for the path with the minimum travel time through Dijkstra's algorithm based on the OD matrices of electric and hydrogen fuel cell vehicles, as shown in Figures 6 and 7.

 doi:10.20944/preprints202311.1594.v1

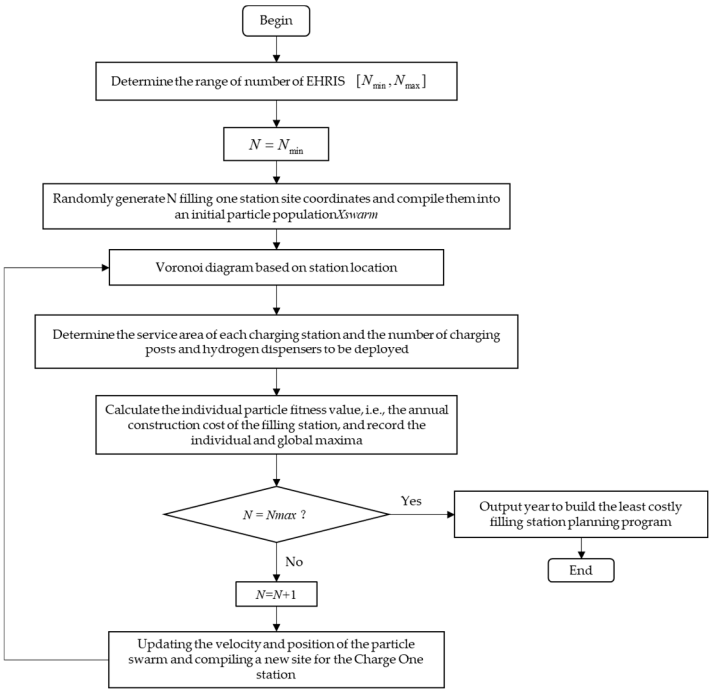

Figure 4. EHRIS solving flow chart.

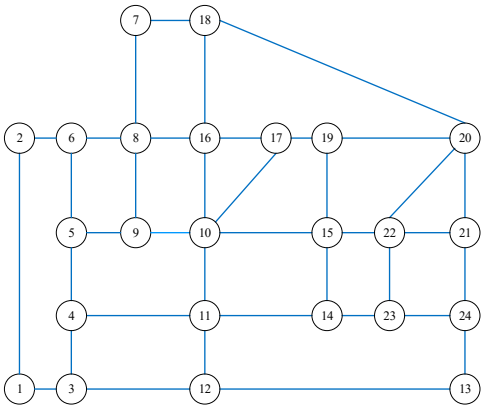

Figure 5. Sioux Falls network topology diagram.

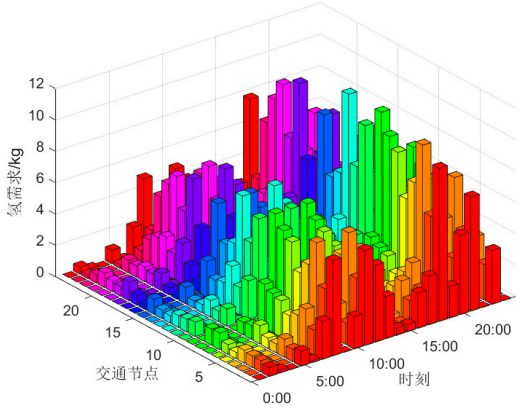

Figure 6. Hydrogen load demand distribution in transportation.

 doi:10.20944/preprints202311.1594.v1

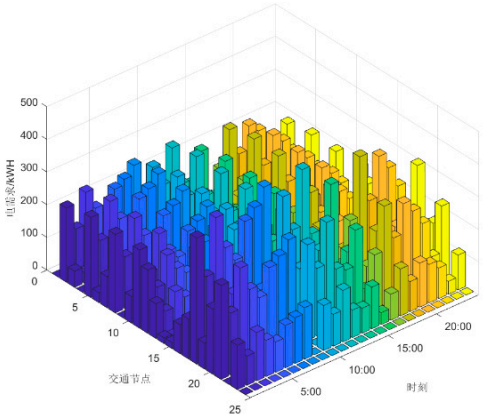

Figure 7. Electric load demand distribution in traffic.

As can be seen from Figure 6, the main time distribution of hydrogen demand for hydrogen fuel cell vehicles peaks at 12:00-13:00 and 21:00-23:00, mainly due to the fact that hydrogen fuel cell vehicle users focus on hydrogen injection at the time of returning from noon and returning from work. Hydrogen fuel cell vehicles have a short hydrogen injection time, which is negligible compared to the charging time of electric vehicles, and the number of hydrogen fuel cell vehicles is small compared to the number of electric vehicles in practice. The construction cost of charging equipment for electric vehicles is less, and the construction cost of hydrogen injection equipment for hydrogen fuel cell vehicles is high, and there are many hydrogen production links. Figure 7 shows that the charging behavior of electric vehicles is more random, and the electric load distribution of electric vehicles is more intensive compared to the hydrogen load demand of hydrogen fuel cell vehicles.

7.2. Simulation results

Based on the loads of electric vehicles and hydrogen fuel cell vehicles, the electric-hydrogen refueling stations in Sioux Falls are selected for capacity planning. Set the number of particle population species as 20, $T_{\max}$ is set to be 300 and the number of electric-hydrogen charging stations in the planning area is set as 3~20, and this number of electric-hydrogen charging stations are solved by traversing, and the simulation results are shown in Figure 8 and Table 3, and the two algorithms are iterated as the iteration process in Figure 9.

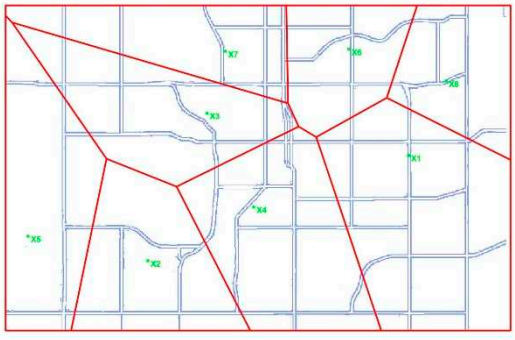

Figure 8. Schematic diagram of planning results.

Preprints.org (www.preprints.org) | NOT PEER-REVIEWED | Posted: 25 November 2023 doi:10.20944/preprints202311.1594.v1

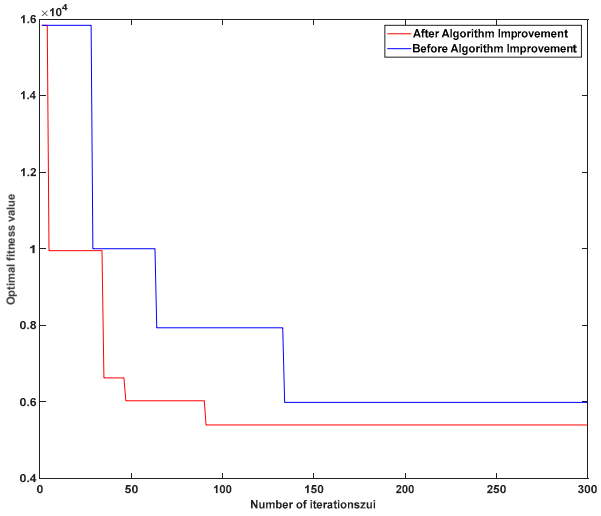

Figure 9. Iterative process.

When the optimal solution occurs when the number of hydrogen charging stations ranges from 7 to 10, the corresponding comprehensive annual social costs of hydrogen charging stations are shown in Table 2. From Table 2, it can be seen that with the increase of the number of hydrogen charging stations, the annual construction cost of hydrogen charging stations is increasing, and the fixed investment cost and operation and maintenance cost of hydrogen charging stations increase accordingly, and because the number of vehicles in the region is fixed, the cost of charging and refueling is similar to the cost of the user's road wear and tear. However, due to the increase in the number of hydrogen charging stations, the loss cost of cars traveling to hydrogen charging stations gradually decreases, and when eight hydrogen charging stations are built in the planning area, the total economic cost of hydrogen charging stations is the lowest, which is ¥53.9867 million.

Table 2. Comprehensive annual economic construction cost of electricity-hydrogen charging integrated station.

Quantities	C_1 ($\times 10^6$ ¥)	C_2 ($\times 10^6$ ¥)	C_3 ($\times 10^6$ ¥)	C_4 ($\times 10^6$ ¥)	C ($\times 10^6$ ¥)
7	5063.76	263.19	39.7	24.73	5399.48
8	5083.92	249.19	35.38	22.08	5398.67
9	5115.72	250.78	38.18	22.34	5435.62
10	5153.09	257.65	31.43	21.8	5472.57

Table 3. Configuration parameters of each charging integrated station.

NHRIS number	Number of charging piles	Number of electrolytic tanks	Hydrogen storage tank capacity/(kg)	Number of hydrogen injectors
X1	17	97	7.9	1
X2	10	96	7.6	1
X3	13	136	11.2	1
X4	23	298	20.1	1
X5	2	19	1.46	1
X6	14	132	10.1	1
X7	27	199	19.4	1
X8	1	7	0.54	1

 doi:10.20944/preprints202311.1594.v1

The eight electric-hydrogen charging stations are numbered from X1 to X8, and the optimal locations of the electric-hydrogen charging stations are shown in Figure 7, and the configurations of charging piles, electrolysis tanks, hydrogen storage tanks, and hydrogen dispensers of each electric-hydrogen charging station are shown in Table 2. Hydrogen fuel cell vehicles account for a low proportion in the transportation field, the number is small, and the hydrogen filling capacity of the hydrogen dispenser is large, one hydrogen dispenser can reach 700 kg of hydrogen per day [30], therefore, only one electric hydrogen charging station can meet the demand for hydrogen filling in the planning area of the city.

7.3. Simulation results

The modified IEEE33 node system is used for the analysis, and the network parameters are detailed in the literature [31]. In this paper, OLTC, ESS, CB, SVC, wind turbine and electric hydrogen charging integrated station are added to the basic network to realize the collaborative planning of the electric hydrogen charging integrated station and the distribution network. The modification is shown in Figure 10. In this case, an OLTC is connected between nodes 33 and 1, node 5, node 15, and node 31 are connected to SVC, node 5 and node 15 are connected to CB, nodes 15 and 32 are connected to the electric energy storage system, and nodes 17 and 32 are connected to the wind farm, respectively. The electric hydrogen production and charging station is connected to nodes 19, 3, 7, 23, 13, 27, 10, and 14, respectively. The wind power and load data in the example are from the actual system. The OLTC ratio range is assumed to be , and the active management equipment parameters are detailed in Appendices Table A2–A4. Literature [32]has demonstrated that the relaxation model with grid losses as the objective function is rigorously accurate, and in addition to this, the objective function of this planning includes the sum of the power purchases from the higher grid. The program is computed in MatlabR2018a environment based on CPLEX 12.8.0 with i5-12400 CPU 2.5GHz,16GB RAM and Win10 64bit operating system.

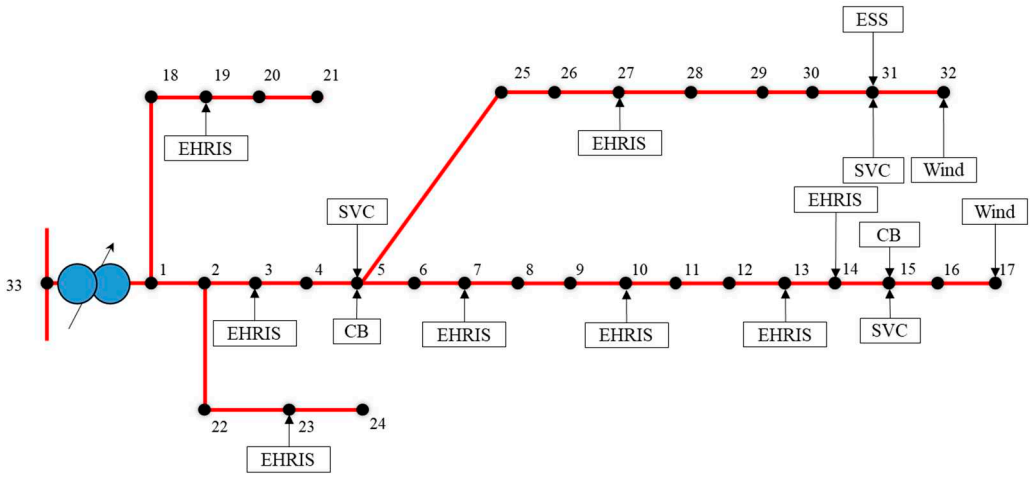

Figure 10. Modified IEEE33 nodes.

According to the original data of the arithmetic example, the active coordination optimization yields the results of each equipment for each time period, as shown in Figures 11–15. Figure 11 shows the 24-hour distribution of the voltage at the IEEE33 node, Figure 12 shows the active output of wind power, and Figures 13 and 14 show the output of reactive power compensator capacitor bank CB and reactive power compensator SVC, respectively.

 doi:10.20944/preprints202311.1594.v1

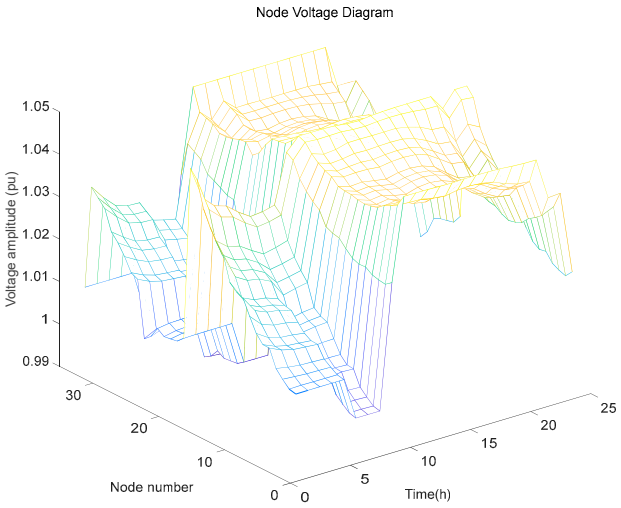

Figure 11. Voltage distribution.

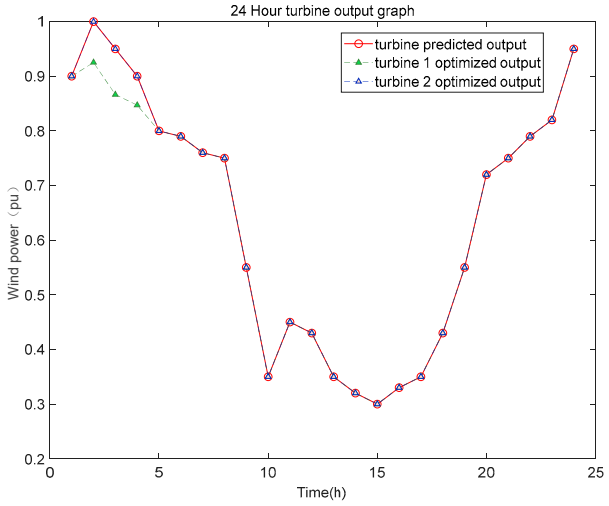

Figure 12. Actual 24-hour turbine output.

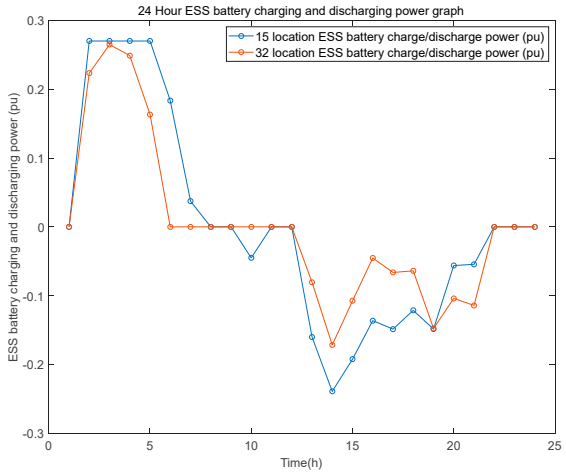

Figure 13. ESS charging and discharging power diagram.

 doi:10.20944/preprints202311.1594.v1

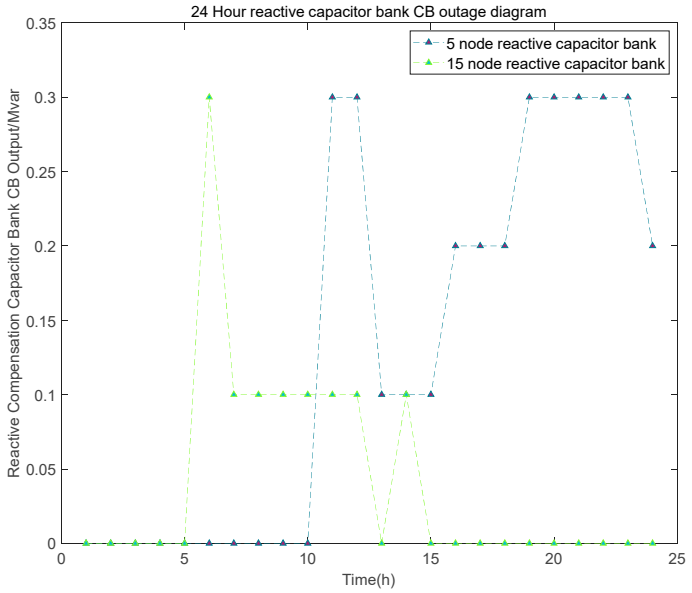

Figure 14. Output diagram of reactive power compensation capacitor bank CB.

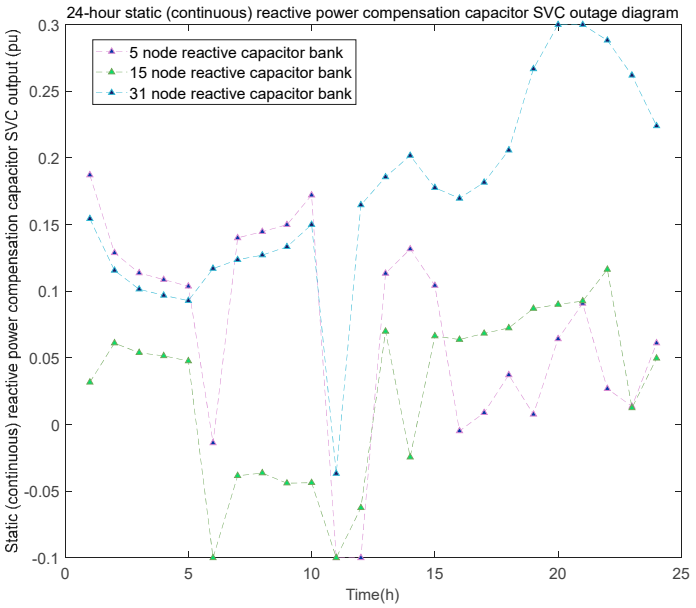

Figure 15. SVC output diagram of reactive power compensator.

From Figures 12–16, it can be seen that: 1) in the load trough section (00:00-04:00), due to the need to ensure the lower limit value of 0.5MW output of the main grid, and the ESS is limited by its capacity, which can't further absorb the excess clean energy, resulting in the occurrence of power abandonment, and the ESS discharges at the peak load stage, which effectively reduces the peak-to-valley difference of the equivalent load; 2) in the time period of wind power output is higher (night time hours), the OLTC increases the voltage with the increase of electricity consumption, and the reactive device absorbs the excess reactive power of the system in the sub-time period, thus avoiding the occurrence of over-voltage.

 doi:10.20944/preprints202311.1594.v1

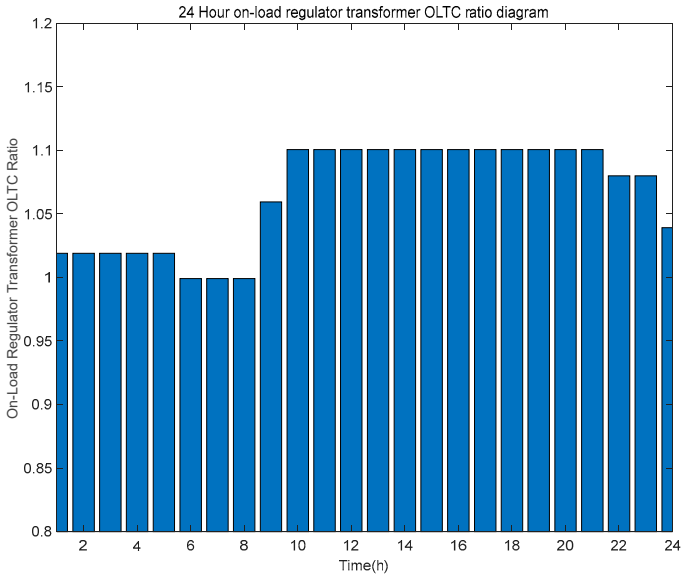

Figure 16. OLTC ratio diagram for on-load regulator transformer.

8. Conclusions

The large-scale promotion of new energy vehicles requires the infrastructure of hydrogen charging stations as a prerequisite, and large-scale integration of new energy vehicles into the grid will have an impact on the power grid. Therefore, in order to meet the demand of hydrogen energy for automobiles, it is necessary to consider the coordinated planning of the hydrogen charging station and the power distribution network. In this paper, the model of hydrogen charging station is designed to minimize the total social cost in the planning area, and the particle swarm method is used to solve the model for the highly nonlinear characteristics of the model, which contains many variables. The Voronoi diagram of the hydrogen charging station site is the growth point, and the area formed by the growth is the service area of the hydrogen charging station, and the equipment capacity of the hydrogen charging station is determined according to the electric hydrogen demand of EVs and HFCVs in the service area, and the particle swarm algorithm is used to search for the optimal solution of the objective function of the planning of the hydrogen charging station. The calculation results show that:

(1) In this paper, the OD matrix and BPR road resistance function are used to simulate the travel trajectories of electric vehicles and hydrogen fuel cell vehicles, and the electric hydrogen demand of electric vehicles and hydrogen fuel cell vehicles is obtained by dynamically updating the state parameters of electric vehicles and hydrogen fuel cell vehicles in real time, and the calculation results show that there is an obvious difference in the spatial and temporal distribution of electric loads and hydrogen loads of electric vehicles and hydrogen fuel cells.

(2) This paper establishes an active management model on the basis of planning the electric-hydrogen charging integrated station, and verifies through example simulation that it meets the energy demand of electric vehicles and hydrogen fuel cell vehicles while ensuring the safe and reliable operation of the power grid, and realizes the coordinated planning of the electric-hydrogen charging integrated station and the power distribution grid. In this paper, the spatial and temporal distribution of automobile energy demand is obtained by superimposing the demand of a single quantity of automobiles, and the planning of the integrated electric hydrogen charging station is carried out on the basis of obtaining the electric hydrogen energy demand of automobiles. Finally, by introducing reactive power compensation components and energy storage devices, the grid node voltage is maintained within a % deviation during peaks and valleys, which ensures the safe and reliable operation of the system.

 doi:10.20944/preprints202311.1594.v1

Author Contributions: project administration, Xueqin Tian; methodology, writing—review and editing, Heng Yang; su-pervision, Yangyang Ge; formal analysis and resources, Tiejiang Yuan.

Conflicts of Interest: The authors declare no conflict of interest.

Appendix A

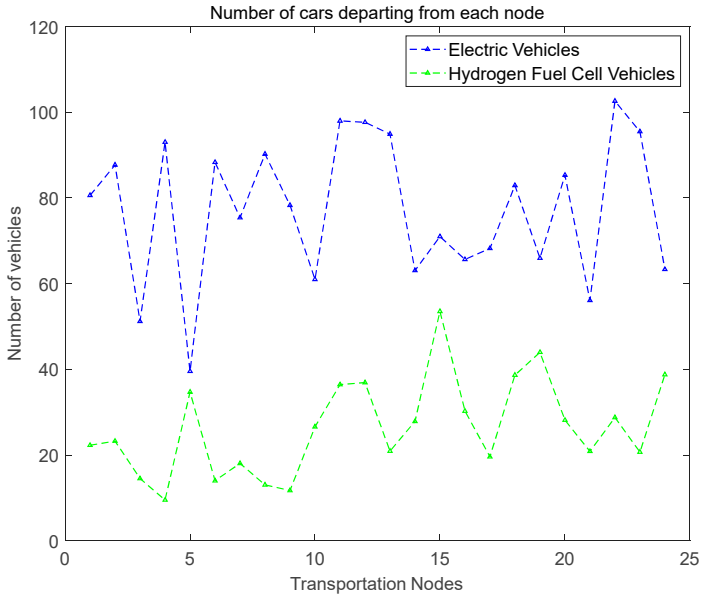

Figure A1. Number of starting cars at each transportation node.

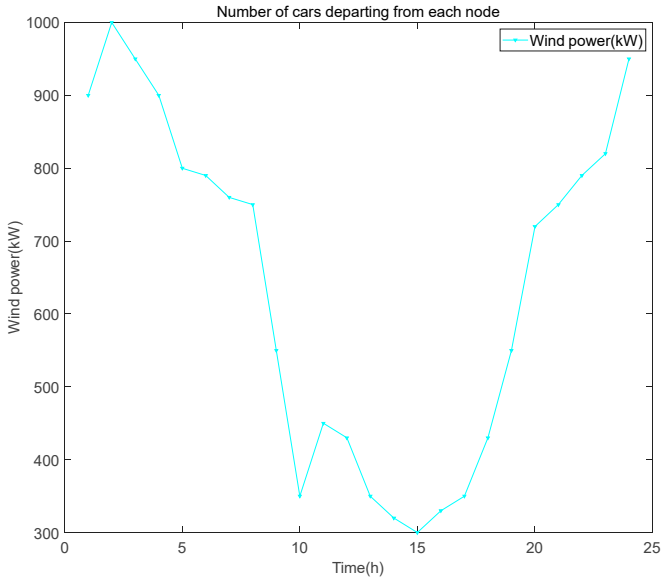

Figure A2. Wind turbine power curve.

 doi:10.20944/preprints202311.1594.v1

Table A1. Tariffs for different time periods.

	Peak Period	Level Period	Valley Period
Time	(12：00-15：00) (20：00-23：00)	(9:00-12:00) (15:00-20:00) (23:00-0:00)	(0：00-9：00)
price of electricity （¥/kWh）	0.56	0.39	0.30

Table A2. Parameters of CB.

Nodes	Unit capacity /Mvar	Quantities
5、31	0.01	5

Table A3. Parameters of ESS.

Nodes	Limit of power /MW	Limit of capacity/($\mathrm{MW \cdot h}$)	Charging efficiency	Discharging efficiency
15、32	0.3	1.5	0.9	1.11

Table A4. Parameters of SVC.

Nodes	Compensation coverage
5、15、31	[-0.1,0.3]

References

1. Mahmud, N.; Zahedi, A.J.R.; Reviews, S.E. Review of control strategies for voltage regulation of the smart distribution network with high penetration of renewable distributed generation. **2016**, *64*, 582-595.
2. Manoharan, Y.; Hosseini, S.E.; Butler, B.; Alzhahrani, H.; Senior, B.T.F.; Ashuri, T.; Krohn, J. Hydrogen fuel cell vehicles; current status and future prospect. *Applied Sciences* **2019**, *9*, 2296 %@ 2076-3417.
3. Xu, H.; Miao, S.; Zhang, C.; Shi, D. Optimal placement of charging infrastructures for large-scale integration of pure electric vehicles into grid. *International Journal of Electrical Power & Energy Systems* **2013**, *53*, 159-165 %@ 0142-0615.
4. Su, S. Method of Location and Capacity Determination of Intelligent Charging Pile Based on Recurrent Neural Network. *World Electric Vehicle Journal* **2022**, *13*, 186 %@ 2032-6653.
5. Awasthi, A.; Venkitusamy, K.; Padmanaban, S.; Selvamuthukumaran, R.; Blaabjerg, F.; Singh, A.K. Optimal planning of electric vehicle charging station at the distribution system using hybrid optimization algorithm. *Energy* **2017**, *133*, 70-78 %@ 0360-5442.
6. Yang, G.; Jiang, Y.; You, S. Planning and operation of a hydrogen supply chain network based on the off-grid wind-hydrogen coupling system. *International Journal of Hydrogen Energy* **2020**, *45*, 20721-20739 %@ 20360-23199.
7. Sun, H.; He, C.; Wang, H.; Zhang, Y.; Lv, S.; Xu, Y. Hydrogen station siting optimization based on multi-source hydrogen supply and life cycle cost. *International journal of hydrogen energy* **2017**, *42*, 23952-23965 %@ 20360-23199.
8. Kuby, M.; Lines, L.; Schultz, R.; Xie, Z.; Kim, J.-G.; Lim, S. Optimization of hydrogen stations in Florida using the flow-refueling location model. *International journal of hydrogen energy* **2009**, *34*, 6045-6064 %@ 0360-3199.
9. Gu, J.; Wang, C.; Xie, D. Research on optimal operation of electricity-hydrogen integrated station in electricity market environment. *Journal of Electric Power Science and Technology* **2022**, *37*, 130-139 %@ 1673-9140.
10. Gao, C.; Wang, W.; Chen, T. Capacity Planning of Electric-hydrogen Integrated Energy Station Based on Reversible Solid Oxide Battery. *Zhongguo Dianji Gongcheng Xuebao/Proceedings of the Chinese Society of Electrical Engineering* **2022**, *42*, 6155-6169, doi:10.13334/j.0258-8013.pcsee.211634.
11. LeBlanc, L.J.; Morlok, E.K.; Pierskalla, W.P. An efficient approach to solving the road network equilibrium traffic assignment problem. *Transportation research* **1975**, *9*, 309-318 %@ 0041-1647.

12. Chen, M.; Lu, H.; Chang, X.; Liao, H. An optimization on an integrated energy system of combined heat and power, carbon capture system and power to gas by considering flexible load. *Energy* **2023**, *273*, 127203, doi:https://doi.org/10.1016/j.energy.2023.127203.
13. Xue, P.; Zhao, B.; Zhang, L.; Deng, M.; Liu, J.; Huang, Y.; He, Z. Planning Method for Electric Vehicle Charging Station Considering Reliability Constraint. In Proceedings of the 2023 Panda Forum on Power and Energy (PandaFPE), 27-30 April 2023, 2023; pp. 1557-1561.
14. Chen, Z.; Chen, Y.; Che, S. Framework of Integrated Charging Station for Renewable Energy Vehicle and Energy Optimal Dispatching Method. *Dianli Xitong Zidonghua/Automation of Electric Power Systems* **2019**, *43*, 41-49, doi:10.7500/AEPS20181110001.
15. Chen, L.; Yang, F.; Xing, Q.; Wu, S.; Wang, R.; Chen, J. Spatial-temporal distribution prediction of charging load for electric vehicles based on dynamic traffic information. In Proceedings of the 4th IEEE Conference on Energy Internet and Energy System Integration, EI2 2020, October 30, 2020 - November 1, 2020, Wuhan, China, 2020; pp. 1269-1274.
16. Chen, L.; Zhang, Y.; Figueiredo, A. Charging load forecasting of electric vehicles based on multi-source information fusion and its influence on distribution network. *Dianli Zidonghua Shebei/Electric Power Automation Equipment* **2018**, *38*, 1-10, doi:10.16081/j.issn.1006-6047.2018.12.001.
17. Iliopoulou, C.; Kampitakis, E.; Kepaptsoglou, K.; Vlahogianni, E.I. Dynamic traffic-aware auction-based signal control under vehicle to infrastructure communication. *Physica A: Statistical Mechanics and its Applications* **2022**, *608*, 128258, doi:https://doi.org/10.1016/j.physa.2022.128258.
18. Zhang, X.; Wang, Z.; Qian, W.; Hu, K.; Zhou, X.; Li, X. Spatio-temporal dynamic load forecasting of charging pile based on spatio-temporal neural network. *Shaanxi Electric Power* **2019**, *47*, 50-54.
19. Yuanshuo, Z.; Feng, L.I.; Jiuling, D. Optimal dispatch strategy of spatio-temporal flexibility for electric vehicle charging and discharging in vehicle-road-grid mode [J]. *Automation of electric power systems* **2022**, *46*, 88-97.
20. Zhang, L.; Xu, C.; Wang, L.; Li, J.; Chen, X.; Yang, X.; Shi, Y. OD matrix based spatiotemporal distribution of EV charging load prediction. *Dianli Xitong Baohu yu Kongzhi/Power System Protection and Control* **2021**, *49*, 82-91, doi:10.19783/j.cnki.pspc.201535.
21. Yu, T.; Ma, J. A review of the link traffic time estimation of urban traffic. In Proceedings of the 2016 IEEE International Conference on Intelligent Transportation Engineering, ICITE 2016, August 20, 2016 - August 22, 2016, Singapore, Singapore, 2016; pp. 123-127.
22. Othman, A.M.; Gabbar, H.A.; Pino, F.; Repetto, M. Optimal electrical fast charging stations by enhanced descent gradient and Voronoi diagram. *Computers and Electrical Engineering* **2020**, *83*, doi:10.1016/j.compeleceng.2020.106574.
23. Li, Y.; Cui, F.; Li, L. An integrated optimization model for the location of hydrogen refueling stations. *International Journal of Hydrogen Energy* **2018**, *43*, 19636-19649, doi:10.1016/j.ijhydene.2018.08.215.
24. Cao, F.; Meng, Q.; Miao, P.; Li, Y. Optimal substation planning based on improved weighted voronoi diagram and genetic algorithm. *Dianwang Jishu/Power System Technology* **2015**, *39*, 511-516, doi:10.13335/j.1000-3673.pst.2015.02.033.
25. Hou, H.; Tang, J.; Wang, Y.; Xia, X.; Wang, F.; Hu, P.; Xie, C. Layout planning of electric vehicle charging stations in urban areas.*Dianli Xitong Baohu yu Kongzhi/Power System Protection and Control* **2022**, *50*, 181-187, doi:10.19783/j.cnki.pspc.226008.
26. Yan, G.; Liu, H.; Han, N.; Chen, S.; Yu, D. An Optimization Method for Location and Capacity Determination of Charging Stations Considering Spatial and Temporal Distribution of Electric Vehicles. *Zhongguo Dianji Gongcheng Xuebao/Proceedings of the Chinese Society of Electrical Engineering* **2021**, *41*, 6271-6283, doi:10.13334/j.0258-8013.pcsee.202001.
27. Gao, H.; Liu, J.; Shen, X.; Xu, R. Optimal Power Flow Research in Active Distribution Network and Its Application Examples. *Zhongguo Dianji Gongcheng Xuebao/Proceedings of the Chinese Society of Electrical Engineering* **2017**, *37*, 1634-1644, doi:10.13334/j.0258-8013.pcsee.152839.
28. Low, S.H. Convex relaxation of optimal power flow - Part i: Formulations and equivalence. *IEEE Transactions on Control of Network Systems* **2014**, *1*, 15-27, doi:10.1109/TCNS.2014.2309732.
29. Zhou, L.; Peng, W.; Ma, L.; Yu, W. Orderly Charging and Discharging Scheduling of DC V2G Charging Pile Considering Load Balance of Electricity Reticulation. In Proceedings of the 1st IEEE International Conference on Applied Intelligence and Sustainable Computing, ICAISC 2023, June 16, 2023 - June 17, 2023, Hybrid, Dharwad, India, 2023.

 doi:10.20944/preprints202311.1594.v1

30. Jiang, Y.; Yang, G.; Zhu, Z. Wind-Hydrogen-Electricity Coupled Network Planning Considering Traffic Flow Capture. *Dianli Xitong Zidonghua/Automation of Electric Power Systems* **2021**, *45*, 19-28, doi:10.7500/AEPS20210303011.
31. Kashem, M.A.; Ganapathy, V.; Jasmon, G.B.; Buhari, M.I. A novel method for loss minimization in distribution networks. 2000; pp. 251-256 %@ 078035902X.
32. Abdelouadoud, S.Y.; Girard, R.; Neirac, F.-P.; Guiot, T. Optimal power flow of a distribution system based on increasingly tight cutting planes added to a second order cone relaxation. *International Journal of Electrical Power & Energy Systems* **2015**, *69*, 9-17 %@ 0142-0615.